Mech Time-Depend Mater (2008) 12: 249–272
DOI 10.1007/s11043-008-9061-x

Mechanical properties of Epon 826/DEA epoxy

Jennifer L. Jordan · Jason R. Foley · Clive R. Siviour

Received: 14 April 2008 / Accepted: 15 July 2008 / Published online: 26 July 2008

Abstract Polymers are becoming increasingly used in aerospace structural applications, where they experience complex, non-static loads. Correspondingly, the mechanical properties at high strain rates are of increasing importance in these applications. This paper investigates the compressive properties of Epon 826 epoxy resin cured with diethynolamine (DEA) across strain rates from 10^{-3} to 10^{4} s^{-1}. Specimens were tested using an Instron mechanical testing machine for static loading, traditional split Hopkinson pressure bars (SHPBs) for high strain rates, and a miniaturized SHPB for ultra-high strain rates. Additionally, the material was tested using dynamic mechanical analysis to determine the effects of time and temperature equivalences on the strain rate behavior of the samples. The experimental data is used to fit the Mulliken-Boyce model, modified for one-dimension, which is able to capture the compressive mechanical properties over a range of strain rates.

Keywords Glassy polymer · High strain rate mechanical properties · Epoxy · Mulliken-Boyce model

1 Introduction

Impact and high-strain-rate properties of fiber reinforced composites are of increasing interest as their application in commercial and military products becomes widespread. The role of the epoxy binder in these composites is extremely important due to the 'bilinear' dependence of polymers on strain rate. The high-rate, large-strain mechanical properties

J.L. Jordan (✉)
Energetic Materials Branch, Munitions Directorate, Air Force Research Laboratory, Eglin AFB, FL 32542, USA
e-mail: jennifer.jordan@eglin.af.mil

J.R. Foley
Fuzes Branch, Munitions Directorate, Air Force Research Laboratory, Eglin AFB, FL 32542, USA

C.R. Siviour
Department of Engineering Science, University of Oxford, Oxford OX1 3PJ, UK

of polymers are greatly affected by both strain rate and temperature. The first study of the stress-strain behavior of polymers over a wide range of strain rates is usually regarded as being that of Chou et al. (1973), who examined the behavior of polymethyl methacrylate (PMMA), cellulose acetate butyrate, polypropylene and nylon 66, in compression, using a 'medium strain-rate machine' and a split Hopkinson pressure bar (SHPB) (Chou et al. 1973). While it was expected that the stress supported at a given strain would be a linear function of $\log(\dot{\varepsilon})$, where $\dot{\varepsilon}$ is the strain rate, a bilinear dependence was found with increased slope at high strain rates. This behavior was also observed by Briscoe and Hutchings (1976) and Kukureka and Hutchings (1981) for high density polyethylene (HDPE). However, doubt was cast on the validity of the measurements by Briscoe and Nosker, who considered carefully the effects of friction and specimen response in the Hopkinson bar (Briscoe and Nosker 1984, 1985), and Brown et al. (2007), who investigated several forms of polyethylene (PE). They concluded that in fact the yield strength of HDPE is linear with $\log(\dot{\varepsilon})$.

Walley and Field (1994) examined the behavior of a large number of polymers, at room temperature and strain rates ranging from 10^{-2} to 10^{4} s^{-1}, taking great care to use suitable lubrication and specimen sizes to reduce friction and inertia. Again, they plotted the yield stress as a function of $\log(\dot{\varepsilon})$, and found that the polymers tested fell into three distinct groups:

- A linear relationship, with no change at higher strain rates, such as acetal, HDPE, and dry nylon 6.
- A bilinear behavior with a sharp increase in gradient at a strain rate of $\sim 10^{3}$ s^{-1}, such as polypropylene (PP), polyvinyl chloride (PVC), and polyvinylidine fluoride (PVDF).
- A decrease in maximum stress at a strain rate of $\sim 10^{3}$ s^{-1}, possibly followed by an increase, such as dry nylon 66, polycarbonate (PC), and polyetheretherketone (PEEK).

In addition to strain rate, temperature has an important effect on the mechanical properties of polymers. Bauwens-Crowet conducted a series of compression experiments on PMMA at rates between 10^{-4} and 1 s^{-1} (Bauwens-Crowet 1973). Each of these rate sweeps was repeated every 20°C between −20 and 100°C. The dependence of yield stress on strain rate and temperature was reported, and time and temperature equivalences extended the range of the experiments to 10^{6} s^{-1} at 100°C. In addition, the material was tested at a strain rate of 4×10^{3} s^{-1} over a range of temperatures. Both sets of data showed a bilinear relationship, with increased strength at high strain rates and at low temperatures. In earlier papers, Bauwens and colleagues had investigated PC in compression over a range of temperatures, and found a similar relationship (Bauwens-Crowet et al. 1972; Bauwens 1972). This behavior was attributed to the different molecular relaxations in the material. At high temperatures or low strain rates only the α relaxation (glass transition) plays a role in the polymer behavior, whilst at low temperatures or high strain rates, the effect of the β relaxation is added to that of the α. The authors developed a model to explain the yield stressbehavior, which was also used by Rietsch and Bouette (1990). More recently, Siviour et al. (2005, 2006) performed experiments on PC and PVDF. Using temperature-strain rate equivalence, they identified how the different transitions affected the strain rate dependence of material strength. Mulliken and Boyce (2006) further showed how shifting data from dynamic mechanical analysis (DMA) curves can be used to develop the physically based understanding behind a predictive model for high strain rate behavior of polymers.

Although there is a large body of literature on the mechanical and thermal properties of epoxy (Buckley et al. 2001, 2004; Khan et al. 2002; Gilat et al. 2007), even with the same

epoxy resin, the properties can vary greatly with curing agent (Kozey and Kumar 1994; Miwa et al. 1995) and curing regime (Kozey and Kumar 1994). The mechanical properties of Epon 826 and Epon 828, a similar resin, have been studied by several authors (Katz et al. 1980; Enns and Gillham 1983; Truong 1990; Kozey and Kumar 1994; Miwa et al. 1995; Chen and Zhang 1997; Chen and Zhou 1998; Chin et al. 1998; Lu et al. 2001; Hu et al. 2003; Xia et al. 2003). Hu et al. (2003) and Xia et al. (2003) found that under shear loading Epon 826 cured with Epi-cure 9551 exhibited strain rate dependence, with no dependence on hydrostatic pressure up to 17 MPa. Chen and Zhang (1997) and Chen and Zhou (1998) studied Epon 828 with curing agent T-403 under compressive loading at a range of strain rates and temperatures. They found a bilinear rate dependence similar to that shown in the Walley and Field study (Walley and Field 1994). Additionally, the compressive yield strength showed a strong dependence on the test temperature.

This paper presents results from recent experiments investigating the quasi-static and high strain rate compressive properties of Epon 826 epoxy resin cured with diethanolamine (DEA) hardener. The effects of time—temperature equivalence on the mechanical properties of the epoxy material are investigated. The Mulliken-Boyce (Mulliken 2004, 2006; Mulliken and Boyce 2006; Mulliken et al. 2006) model, which has been used to describe PC, PMMA, and PVC, is translated from 3-D to 1-D and applied to the epoxy material in this study.

2 Experimental procedure

2.1 Sample preparation

The Epon 826 resin (100 parts by weight) was mixed with the DEA hardener (12 parts by weight) and cast into a large rectangular pan. The epoxy was cured at 80°C for 12 hours. After curing, samples for testing were machined from the large block of material.

2.2 Experimental set-up

Dynamic mechanical analysis was performed in a single cantilever configuration at 1, 10, and 100 Hz over temperatures from 148 K to 473 K.

Compression experiments were performed across a range of strain rates from 10^{-2} to 10^{4}, at room temperature and at 1470 s^{-1} across a range of temperatures (213–333 K). An Instron model 2630 was used for quasi-static loading, in which the cylindrical samples were nominally 8 mm diameter by 3.5 mm thick. It is generally accepted that quasi-static compression samples should have a length to diameter ratio of 2:1. However, it has been shown that there is little difference between samples tested quasi-statically using 2:1 or 1:2 length:diameter ratio (Chen and Zhang 1997). In these experiments, samples with dimensions identical to those used for the split Hopkinson pressure bar were tested. The strain in the sample was determined from crosshead displacement, and the stress was determined from the load cell output. All data was acquired using Instron's Merlin software.

Experiments at 10 and 100 s^{-1} were performed in a Hydraulic loading system at the University of Oxford, which was also used to repeat experiments at 1 s^{-1} to provide overlap between the techniques. In this device, the specimen is placed between two anvils, one attached to a hydraulic piston and the other to a short strain gage based load cell. Loading is provided by driving the piston into the specimen at a pre-set speed over a pre-set distance. The change in specimen length is measured using LVDTs mounted on the loading anvils.

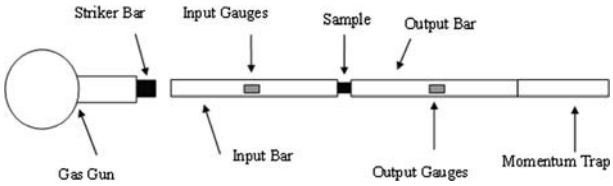

Fig. 1 Schematic of split Hopkinson pressure bar (SHPB) experimental set-up

Table 1 Selected properties of the bar materials used in the SHPB and MSHPB. Density, acoustic wave speed, and impedance are measured from the bar materials. Yield stresses are literature values

Material	Density ρ (kg/m^3)	Wave speed (acoustic) c (mm/μs)	Impedance (acoustic) $Z = \rho c$ ($\times 10^7$ kg m^{-2} s^{-1})	Yield stress σ_Y (MPa)
440-HT stainless steel	6157	5.542	3.41	1970
6061-T6 Al	2716	5.039	1.36	290
British Maraging Steel	8082	4.835	3.90	758
WC	14527	6.316	9.18	2600
Ti6Al4V	2709	5.039	1.37	1000

The stress-strain relationship in the specimen is calculated from the change in length and the supported load. The piston can be driven at speeds up to ∼2 ms^{-1}; however, the inertia of the LVDTs limits displacement, and thus strain accuracy at strain rates above, typically, ∼50 s^{-1}, although force, and therefore stress, are still accurately recorded at these rates.

Compression experiments at intermediate strain rates (10^3–10^4) were conducted using two split Hopkinson pressure bars (SHPB) (Tasker et al. 1998; Gray III 2002), a schematic diagram of which can be seen in Fig. 1. The experiments varying strain rate were conducted using the SHPB system located at AFRL/RWME, Eglin AFB, FL, which is comprised of 1524 mm long, 19 mm diameter incident and transmitted bars of 440-HT stainless steel or 6061-T6 aluminum. The striker is 305 mm long and made of the same material as the other bars. The samples, which were nominally 8 mm diameter by 3.5 mm thick or 5 mm diameter by 2.5 mm thick, depending on strain rate, are positioned between the incident and transmitted bars. The bar faces were lightly lubricated with paraffin wax to reduce friction (Trautmann et al. 2005).

The experiments varying temperature were performed using the SHPB system at the Cavendish Laboratory, University of Cambridge, which consists of 500 mm long, 12.7 mm diameter incident and transmitted bars with a 200 mm striker bar of grade 300 maraging steel. The sample, which is the same size as those tested in the Eglin bars, is contained in an environmental chamber. Temperature is varied by flowing heated or cooled helium gas through the chamber until the desired temperature is reached. Temperature measurements are made with a thermocouple mounted on the end of the bar close to the sample. The measured temperature represents the sample temperature to ±0.5°C.

The properties of the stainless steel, aluminum, and maraging steel bars are given in Table 1.

Experiments at ultra-high strain rates (10^4 s^{-1}) were conducted using a miniaturized split Hopkinson pressure bar (MSHPB), which is, in principle, identical to the full sized SHPB. However, the bars are 300 mm long and 3–3.2 mm in diameter. Samples tested in this apparatus are nominally 1.5 mm diameter by 0.6 mm long. Miniaturized direct impact bar

systems have been widely studied (Gorham 1979; Mentha et al. 1984; Gorham et al. 1992) and Jia and Ramesh (2004) published a comprehensive analysis of a similar miniature bar system. A major advantage of the split bar system, over direct impact, is that mechanical equilibrium in the specimen may be conformed by comparing one- and two-wave analyses, as described by Gray III (2002). The MSHPB, at Eglin AFB, provides the opportunity to test materials up to strain rates of 10^5 s^{-1}, with tungsten carbide (WC) and titanium alloy (Ti-6Al-4V) bar materials available. The properties of these bar materials are also listed in Table 1.

For all bar systems, the properties of the sample are determined by measuring the incident, reflected, and transmitted strain signals, ε_I, ε_R, and ε_T respectively, using Kulite AFP-500-90 semiconductor strain gages. These gages are smaller (1 mm long) than traditional foil gages and have a much higher gage factor (140). The gages form part of a potential divider circuit with constant voltage excitation, which transforms the resistance change of the gages to a voltage change and compensates for temperature changes. The strain gages are dynamically calibrated in situ by performing a number of impacts with carefully measured striker bar velocities. From the measured impact velocity and mass of the striker, the force amplitude of the stress pulse introduced, F, can be determined and compared to the voltage output, V, from the strain gages to give a calibration in the form:

$$F = KV(1 + bV), \tag{1}$$

where K and b are calibration factors.

The full derivation of the data reduction used to calculate the strain rate and stress in the specimen, as functions of time, can be found in references (Tasker et al. 1997, 1998; Gray III 2002). In order to make representative measurements of material properties, it is necessary that the specimen achieves mechanical equilibrium during the experiment, and this is sometimes assumed as it makes the strain rate calculation more straightforward (Gray III 2002). Equilibrium can be confirmed in practice by calculating the stresses on the front and rear faces of the specimen using the one- and two-wave analyses, respectively, as described by (Gray III 2002). The software used in the experiments presented in this paper performs the one- and two- wave analyses automatically for every specimen, so stress state equilibrium is verified in every experiment. However, the calculation of strain rate does not assume mechanical equilibrium, rather it uses all three of the incident, reflected and transmitted force pulses to calculate specimen strain rate through the following equation:

$$\dot{\varepsilon}(t) = \left[\frac{C_b}{l_S}\right](\varepsilon_I(t) - \varepsilon_R(t) - \varepsilon_T(t)), \tag{2}$$

where ε_I, ε_R, and ε_T are the incident, reflected and transmitted strain pulses time shifted to the front and rear faces of the specimen, respectively, C_b is the sound speed in the bar material, and l_S is the length of the sample. This specimen strain rate is then integrated to give the strain,

$$\varepsilon(t) = \int_0^t \dot{\varepsilon}(t)dt, \tag{3}$$

and the transmitted strain pulse is used to calculate the reported one-wave specimen stress,

$$\sigma(t) = \left[\frac{E_b A_b}{A_S}\right]\varepsilon_T(t), \tag{4}$$

where E_b, and A_b are the elastic modulus and cross-sectional area of the bar material, respectively, and A_S is the cross-sectional area of the sample. The two-wave specimen stress is calculated using (4) with ε_T replaced by $\varepsilon_I + \varepsilon_R$. If true stress is required, A_S is typically updated using the strain calculation, assuming that volume is conserved during deformation.

2.3 Description of the model

The Mulliken-Boyce model, based on previously developed models by Boyce et al. (Boyce et al. 1988; Arruda and Boyce 1993; Bergstrom and Boyce 1998; Boyce et al. 2000, 2001), is a three-dimensional rate-, temperature- , and pressure-dependant model for thermoplastic polymers. The model, described one-dimensionally in Fig. 2, is composed of two parts: (A) linear elastic springs and viscoelastic dashpots in series and (B) a non-linear Langevin spring. The linear springs and dashpots represent intermolecular resistance to chain segment rotation, and the Langevin spring represents entropic resistance to chain alignment. The linear springs and dashpots are further decomposed into α and β. The α process relates to rotation of main-chain polymer segments, and the β process, in epoxy, relates to relaxations of glyceryl or diphenylpropane groups [33, 34].

Although the Mulliken-Boyce model is a full three-dimensional model appropriate for implementation in a finite element code, such as ABAQUS, in this work the model was adapted to one dimension and implemented in MatLAB. Since the available data from this study was compressive stress-strain curves at varying rates and temperatures, this simplification allowed for understanding how the model could be applied to epoxy and permitted optimization of the model parameters using genetic algorithm, available in MatLAB.

The stress, $\sigma_i (i = \alpha, \beta)$, in the elastic spring is proportional to the strain, ε^e

$$\sigma_\alpha = E_\alpha \varepsilon^e, \tag{1a}$$

$$\sigma_\beta = E_\beta \varepsilon^e \tag{1b}$$

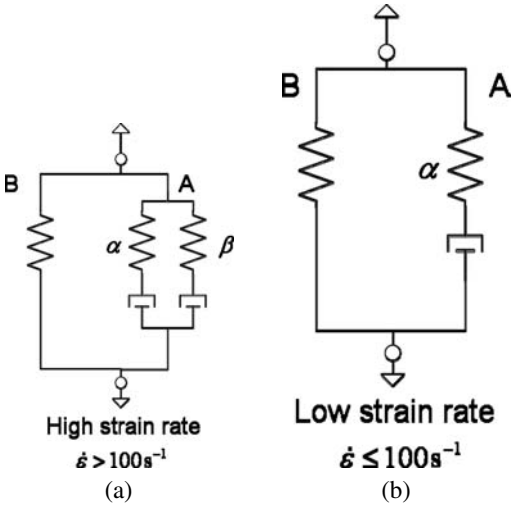

Fig. 2 Schematic of (**a**) a one-dimensional Mulliken-Boyce model (Mulliken 2004, 2006; Mulliken and Boyce 2006; Mulliken et al. 2006) for glassy polymers. For low strain rates ($\dot{\varepsilon} < 100\ s^{-1}$), the modified model in (**b**) neglects the contribution of the β transition

where E_i is the temperature and rate dependant Young's modulus. The shear strain rate, $\dot{\gamma}_i^p$ in the viscoplastic dashpots is related to the shear stress, τ_i, by

$$\dot{\gamma}_\alpha^p = \dot{\gamma}_{0,\alpha}^p \exp\left[-\frac{\Delta G_\alpha}{k\theta}\left(1 - \frac{\tau_\alpha}{s_\alpha + \alpha_{p,\alpha} p}\right)\right], \tag{2a}$$

$$\dot{\gamma}_\beta^p = \dot{\gamma}_{0,\beta}^p \exp\left[-\frac{\Delta G_\beta}{k\theta}\left(1 - \frac{\tau_\beta}{s_\beta + \alpha_{p,\beta} p}\right)\right] \tag{2b}$$

where $\dot{\gamma}_{0,i}^p$ is proportional to the attempt frequency; ΔG_i is the activation energy; k is Boltzmann's constant; θ is the absolute temperature; p is the pressure; and $\alpha_{p,i}$ is the pressure coefficient. The athermal shear strength, s_i, is related to the shear modulus, μ_i, and evolves toward a preferred state with plastic straining according to

$$\dot{s}_\alpha = h_\alpha\left(1 - \frac{s_\alpha}{s_{ss,\alpha}}\right)\dot{\gamma}_\alpha^p, \tag{3a}$$

$$\dot{s}_\beta = h_\beta\left(1 - \frac{s_\beta}{s_{ss,\beta}}\right)\dot{\gamma}_\beta^p \tag{3b}$$

with initial conditions

$$s_{0,\alpha} \equiv \frac{0.077\mu_\alpha}{1 - \upsilon_\alpha}, \tag{3c}$$

$$s_{0,\beta} \equiv \frac{0.077\mu_\beta}{1 - \upsilon_\beta} \tag{3d}$$

where h_i is the softening slope, $s_{ss,i}$ is the "preferred state", and ν_i the Poisson's ratio. The shear stress can be scaled by $\sqrt{3}$ and the shear strain by $\frac{1}{\sqrt{3}}$ to relate them to the normal stress and strain, respectively.

The elastic and viscoplastic elements are combined linearly for each component, α and β

$$\dot{\varepsilon}_\alpha = \dot{\varepsilon}_\alpha^e + \dot{\varepsilon}_\alpha^p, \tag{4a}$$

$$\dot{\varepsilon}_\beta = \dot{\varepsilon}_\beta^e + \dot{\varepsilon}_\beta^p \tag{4b}$$

and combined with (1) and rearranged to determine the total stress rate

$$\dot{\sigma}_\alpha = E_\alpha\left(\dot{\varepsilon} - \dot{\varepsilon}_\alpha^p\right), \tag{5a}$$

$$\dot{\sigma}_\beta = E_\beta\left(\dot{\varepsilon} - \dot{\varepsilon}_\beta^p\right). \tag{5b}$$

Equations (2) and (5) are solved simultaneously as a system of time-dependant differential equations to determine the stress in the α and β components.

The three-dimensional stress in the Langevin spring, $\boldsymbol{T_B}$, the network "back stress" due to entropic resistance to molecular alignment, is defined using the Arruda-Boyce (Arruda and Boyce 1993) 8-chain interpretation of molecular alignment

$$T_B = \frac{C_R}{3}\frac{\sqrt{N}}{\lambda_p^{chain}} L^{-1}\left(\frac{\lambda_{chain}^p}{\sqrt{N}}\right)\bar{B}_B' \tag{6}$$

where C_R is the rubbery modulus, $\sqrt{N}$ is the limiting chain extensibility, λ^p_{chain} is the stretch on a chain in the 8-chain network,

$$\lambda^p_{chain} = \sqrt{\frac{\text{trace}\,\bar{B}}{3}}, \tag{7}$$

$L^{-1}(\frac{\lambda^p_{chain}}{\sqrt{N}})$ is the inverse Langevin function,

$$L\left(\frac{\lambda^p_{chain}}{\sqrt{N}}\right) = \coth\left(\left(\frac{\lambda^p_{chain}}{\sqrt{N}}\right)\right) - \frac{1}{(\frac{\lambda^p_{chain}}{\sqrt{N}})}, \tag{8}$$

and $\bar{B}'_B$ is the deviatoric part of the left isochoric Cauchy-Green tensor. In one dimension, according to Anand and Ames (2006), the "back stress" is defined as

$$\sigma_B = \frac{C_R}{3}\frac{\sqrt{N}}{\lambda^{chain}_p} L^{-1}\left(\frac{\lambda^p_{chain}}{\sqrt{N}}\right)\left[U^2 - U^{-1}\right] \tag{9}$$

with

$$\lambda^p_{chain} = \frac{1}{\sqrt{3}}\sqrt{U^2 + 2U^{-1}} \tag{10}$$

where U is the stretch related to strain by

$$U = \exp\varepsilon. \tag{11}$$

The inverse Langevin function can be approximated as:

$$L^{-1}(x) \approx \begin{cases} 1.31446\tan(1.58986x) + 0.91209x & \text{if } |x| \le 0.84136, \\ \frac{1}{sign(x)-x} & \text{if } 0.84136 \le |x| \le 1. \end{cases} \tag{12}$$

The total stress in the polymer is the sum of the stresses in each branch,

$$\sigma = \sigma_{A\alpha} + \sigma_{A\beta} + \sigma_B. \tag{13}$$

In the initial Mulliken-Boyce model (Mulliken 2004; Mulliken and Boyce 2006), the temperature of the sample was assumed to be constant as the material deformed. However, at high strain rates, where the thermodynamic condition has changed from isothermal to adiabatic, the temperature increase in the sample results in increased thermal softening evidenced in the stress-strain curve. In order to account for this, Mulliken and Boyce (Mulliken 2006; Mulliken et al. 2006) added a temperature rate term to the model. Lu et al. (2001) used a similar term in one dimension, adapted here to include the alpha and beta branches

$$\dot{T} = \frac{1}{\rho C_p}[(\dot{\tau}_\alpha \gamma^p_\alpha + \tau_\alpha \dot{\gamma}^p_\alpha) + (\dot{\tau}_\beta \gamma^p_\beta + \tau_\beta \dot{\gamma}^p_\beta)]. \tag{14}$$

There are sixteen material constants defined in the model, as listed in Table 2. The rate and temperature dependant elastic modulus can be determined from DMA data. As in Mulliken and Boyce, the Poisson's ratio was assumed to be rate and temperature independent. The remaining parameters were determined by fitting the model to experimental compressive data using a genetic algorithm.

Table 2 Initial model parameters for the Mulliken-Boyce model (Mulliken 2004, 2006; Mulliken and Boyce 2006; Mulliken et al. 2006) applied to Epon826/DEA

	Units	Value
$E_\alpha(\theta, \dot{\varepsilon})$	MPa	DMA data
$E_\beta(\theta, \dot{\varepsilon})$	MPa	DMA data
$\nu_\alpha(\theta, \dot{\varepsilon})$		0.38
$\nu_\beta(\theta, \dot{\varepsilon})$		0.38
$\dot{\gamma}_{0,\alpha}$	s^{-1}	2.29×10^{15}
$\dot{\gamma}_{0,\beta}$	s^{-1}	2×10^{6}
ΔG_α	J	3.83×10^{-19}
ΔG_β	J	3.32×10^{-20}
$\alpha_{p,\alpha}$		0.316
$\alpha_{p,\beta}$		0.316
$s_{ss,\alpha}$	MPa	0.58
h_α	MPa	300
C_R	MPa	14.2
N	$m^{-1/2}$	2.3
ρ	kg/cc	1140
C_P	J/kg/C	2000

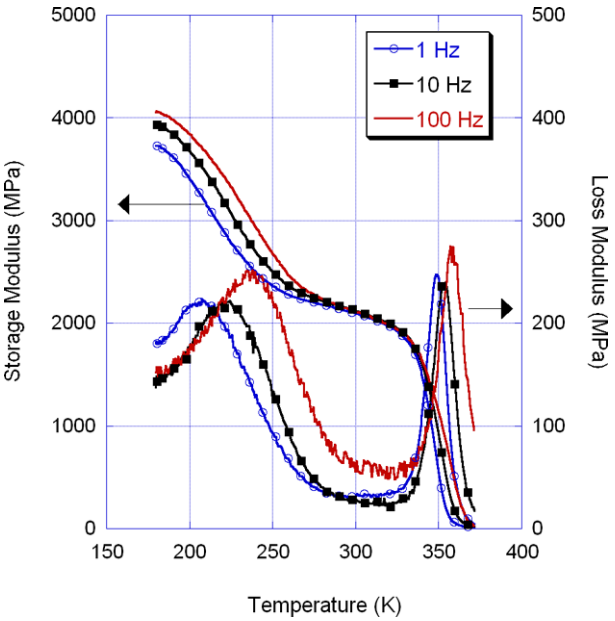

Fig. 3 Dynamic mechanical analysis of epoxy material at 1, 10, and 100 Hz

3 Results and discussion

3.1 Thermomechanical analysis

The storage and loss moduli of the epoxy material were measured using dynamic mechanical analysis, as shown in Fig. 3. It can be seen that there is a glass transition, or α transition, at approximately 350 K. However, the glass transition temperature depends

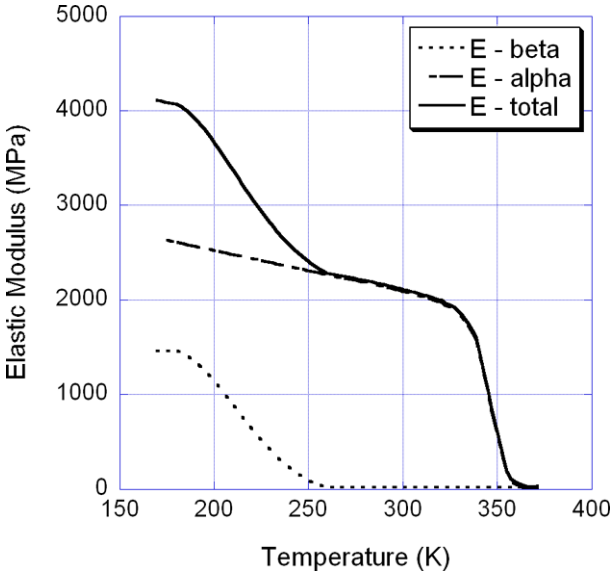

Fig. 4 Elastic modulus of epoxy measured using DMA at 1 Hz ($0.0032\ s^{-1}$) decomposed into α and β components

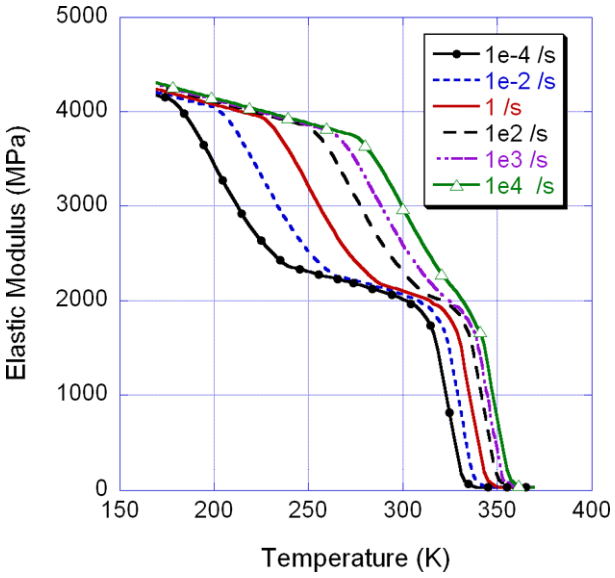

Fig. 5 Elastic modulus of epoxy across a range of strain rates from 1×10^{-4} to $1 \times 10^{4}\ s^{-1}$ predicted using DSR method as described in (Mulliken 2004; Mulliken and Boyce 2006)

on the measurement frequency, with a shift factor of 1.67 K/decade strain rate. Additionally, there is a secondary viscoelastic transition, β, located between 207 and 237 K, which has a much stronger frequency dependence than the glass transition, as shown by the shift factor of 6.59 K/decade strain rate. In other polymer materials, this beta relaxation is found to relate to the molecular mobility of main chain and side groups (Mulliken and Boyce 2006). Specifically, in similar epoxy materials, the beta relaxation is believed to be due to relaxations of glyceryl or diphenlypropane groups (Williams 1979; Foreman et al. 2006).

Using the decompose/shift/reconstruct (DSR) method outlined by Mulliken and Boyce (Mulliken 2004; Mulliken and Boyce 2006), the modulus at strain rates far outside those measured with the DMA can be determined. Using this method, the alpha and beta transitions are decomposed, as shown in Fig. 4. The curve is then shifted to the desired strain rate, using the shift factors detailed above and reconstructed. This was done for a range of strain rates, as shown in Fig. 5. The onset temperature of the β phase transition shifts to near room temperature at strain rates between 1 and 100 s^{-1}, and the contribution of this phase to the overall behavior of the material should become apparent at and above these strain rates.

3.2 Mechanical characterization

Uniaxial compression experiments were conducted on the epoxy material at room temperature across a range of strain rates from 10^{-3} to 10^{4} s^{-1}. The results are presented in Fig. 6, where the curve presented is a representative curve of 3–5 experiments per strain rate. Additional compression experiments were carried out at a constant strain rate, 1470 s^{-1}, and a range of temperatures, as shown in Fig. 7. However, due to the SHPB length used in the temperature tests, the experiment ends shortly after specimen yield. Comparison between the 1×10^{3} room temperature test in Fig. 6 and the 295 K, 1.47×10^{3} test in Fig. 7 reveals a peak stress of approximately 150 MPa. However, the test at temperature in Fig. 7 does not display the entire behavior of that shown in Fig. 6 due to the length of the bars used: the Hopkinson bar system has significantly shorter bars, resulting in a shorter loading period and thus a lower final strain.

Specimen equilibrium in the high strain rate experiments was verified by comparing the one-wave stress, calculated from the transmitted pulse, and the two-wave stress, determined from the incident and reflected pulses, to determine if the two-wave stress oscillates around the one wave stress (Gray III and Blumenthal 2000; Gray III 2002). It can be seen from Fig. 8(a) and (b) that this occurs in samples tested in both the SHPB and the MSHPB, for strain levels well below the peak stress. In both types of experiments, the strain rate increases slightly over the course of the experiment but converting this increase

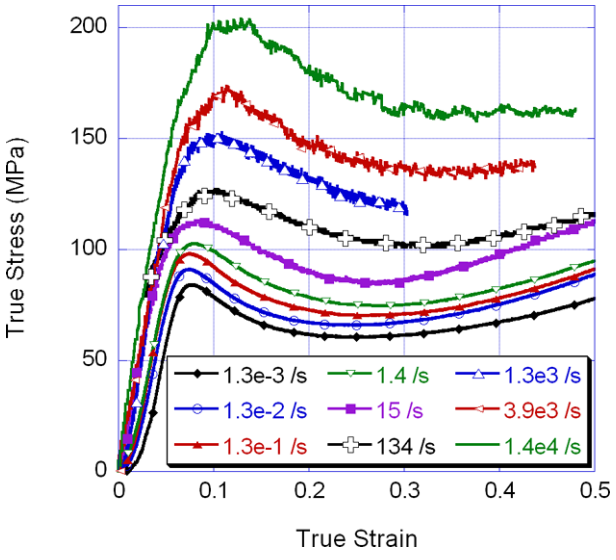

Fig. 6 Compressive stress-strain curves for Epon 826/DEA across a range of strain rates from 10^{-3} to 10^{4}

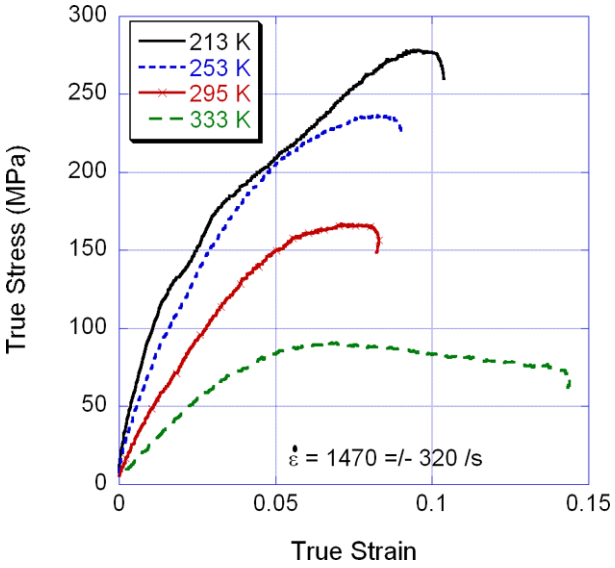

Fig. 7 Effect of temperature on the compressive properties of Epon 826/DEA with changing temperature at a strain rate of 1470 s^{-1}

into $\log(\dot{\varepsilon})$ would show that this is negligible in the context of the material being investigated.

The epoxy material displays a behavior similar to that of other glassy polymers with a linear, then nonlinear rise to peak stress followed by strain softening and then strain hardening at large strains. At about 100 s^{-1}, the thermodynamic condition is changing from isothermal to adiabatic, and thermal softening begins to dominate over strain hardening. At SHPB rates, the test conditions are close to completely adiabatic and increased softening is observed. The SHPB experiments do not go to high enough final strains to fully compare the hardening at large strains.

In order to resolve the strain rate and temperature dependence of the yield stress, the peak stress was plotted against both values in Fig. 9(a) and (b). It can be seen that there is an approximately bilinear dependence of the peak stress on strain rate with the change in slope occurring at $\sim 10^2$ s^{-1}, as predicted from the DSR analysis. However, for the range of temperature tested, the relationship between yield stress and temperature is linear. Based on the modulus curve for 10^3 s^{-1} in Fig. 4, the temperature where one might expect to see a change in slope is right at the top of the range of temperatures tested.

4 Model-based estimation

4.1 Implementation of the Mulliken-Boyce model

Although the Mulliken-Boyce model is a full three-dimensional model appropriate for implementation in a finite element code, such as ABAQUS, in this work the model was adapted to one dimension and implemented in Matlab. Since the available data from this study was compressive stress-strain curves at varying rates and temperatures, this simplification allows the model to be explored for application to epoxy systems.

An additional modification to the Mulliken-Boyce model is made by requiring compressive (positive) stress. If the component stress (particularly in σ_β) is tensile (negative), this

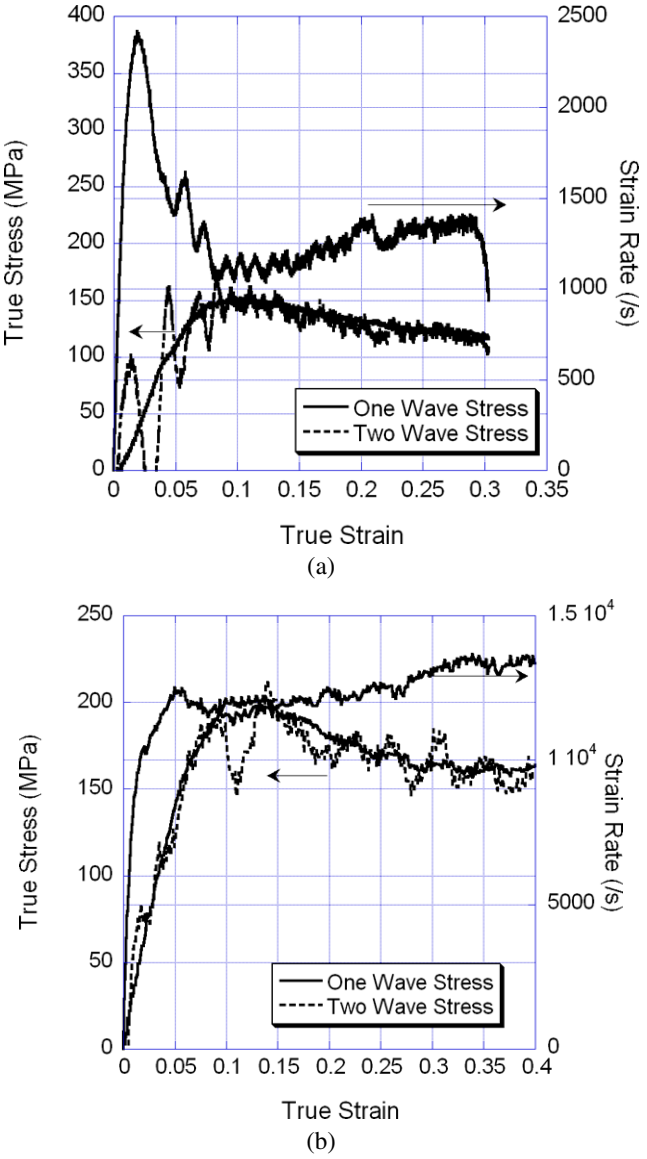

Fig. 8 One-wave versus two-wave stress analysis and strain rate versus strain for (**a**) split Hopkinson pressure bar and (**b**) miniaturized split Hopkinson pressure bar

is considered unphysical and forced to zero. This as the practical effect of defining regimes in strain rate where the effect of the phases are observable. In Fig. 9(a), the transition in the increase of peak stress per decade of strain rate occurs at approximately 100 s^{-1}; this is attributed to the onset of significant β stress contributions. Correspondingly, the β stress predicted by the model is tensile at low strain rates ($\varepsilon < 100$ s^{-1}), which is then forced to zero stress and results only in the α phase contributing, as schematically represented in Fig. 2(b). This definition of model regimes has two immediately obvious benefits: (1) so-

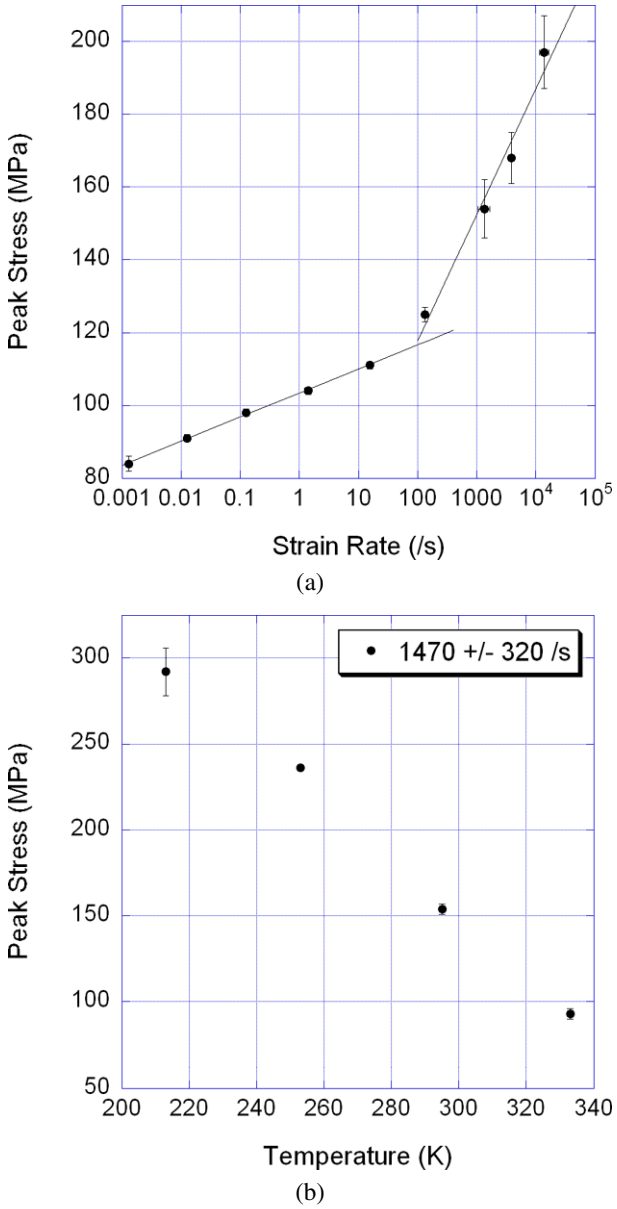

Fig. 9 Peak stress versus (**a**) strain rate and (**b**) temperature for Epon 826/DEA

lutions with unphysical stresses (i.e., tensile β stresses) are prevented, and (2) a sequential approach to the parameter estimation based on the two strain rate domains becomes possible.

Initial estimates for the underlying constitutive model parameters are made using the method outlined by Mulliken (Mulliken 2004; Mulliken and Boyce 2006). The rate dependant elastic springs are described using the rate dependant elastic modulus data determined

from DMA measurements. The Poisson's ratio is determined from ultrasonic sound speed measurements on the sample and is assumed to be constant with temperature and strain rate. The pre-exponential factors and activation energies for the viscoelastic dashpots were determined by separating the yield stress as a function of strain rate into α and β components.

At yield, (2a) and (2b) can be applied to the α and β components, respectively. By solving two simultaneous equations at two different strain rates, both the initial values for the pre-exponential factor and the activation energy can be determined, assuming the pressure coefficients are known. The initial guesses for the pressure coefficients for the viscoelastic dashpots can be determined by comparing compressive and tensile yield strengths, using the tensile data of (Chen et al. 2002). Since limited data was available to determine the pressure coefficient for the β regime, the initial values for the coefficients are assumed to be the same for both components when the β transition is active. Mulliken has reported estimates of the remaining parameters through fits to his experimental data for polycarbonate, which are used for the initial estimates for epoxy.

4.2 Model-based constitutive parameter estimation

Estimating a large number of material constants (in this case, the remaining ten unknown parameters) from a nonlinear model with a limited data set is typical of inverse problems (Alifanov 1994). Due to the noise and variable sensitivity to the parameters, the problem is ill-posed, requiring care in implementation.

It is standard procedure is to utilize all available experimental data, which originates from three different experiments covering a wide range of strain rates (over 7 decades, 0.0013 to 14000 s^{-1}). However, the use of separate experiments to cover the range of strain rates as well the assumption of the two different strain-rate behaviors of the material suggest a sequential estimation approach, outlined in Fig. 10. Estimates for the α-transition parameters and other parameters ($\dot{\gamma}_{0,\alpha}$, ΔG_α, $\alpha_{p,\alpha}$, $s_{ss,\alpha}$, h_α, C_R, and N) are obtained from low strain rate data. The remaining β-stress parameters ($\dot{\gamma}_{0,\beta}$, ΔG_β , and $\alpha_{p,\beta}$) are then estimated from high-strain data, completely determining the unknowns. This approach is essentially a Bayesian approach (Mendenhall 1971; Bar-Shalom et al. 2001) wherein the additional physical parameters that are inactive at low strain rates are then inferred using "new" data from high-strain rate experiments that is sensitive to these parameters.

The properties of the sample are estimated from experimental data using a rigorous model-based estimator. Due to the large number of parameters, stiffness (i.e., solution instability) of the problem, and weak sensitivity to several parameters, use of a robust stochastic

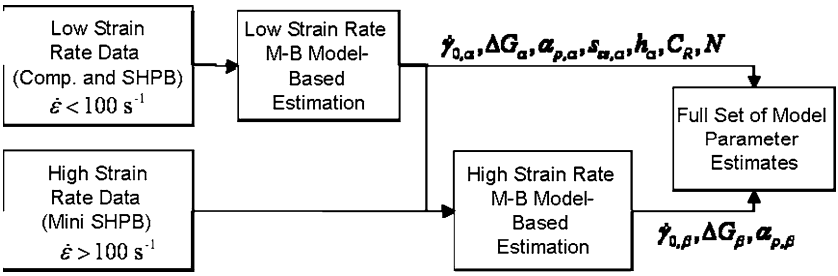

Fig. 10 Flowchart illustrating the use of sequential estimation to first estimate the α-stress contribution and other parameters from low strain rate data and then estimating the β-stress parameters from high-strain data

Table 3 Parameter estimates from the low strain rate data

Symbol	$\dot{\gamma}_{0,\alpha}$	ΔG_α	$\alpha_{p,\alpha}$	$s_{ss,\alpha}$	h_α	C_R	N
Units	s^{-1}	J	–	–	MPa	MPa	$m^{-1/2}$
Min	10^8	10^{-27}	0.1	0.1	1	1	1.3
Initial	1.58×10^{10}	2.51×10^{-19}	0.5	0.518	99	11	2.3
Final	8.45×10^{10}	2.47×10^{-19}	0.236	0.360	117	11.1	1.39
Max	10^{22}	10^{-15}	1	1	800	200	3

estimator is indicated. The robustness to code problems is especially important for regions in the parameter space where the solution to the differential equation is unstable.

The experimental data is processed using the techniques outlined above. Additional preprocessing of the data is performed to eliminate the startup transients in the low strain rate compression tests. These artifacts are negated by independently estimating a zero-strain intercept for the linear region of the data (typically between 25 and 40 MPa stress) and then applying a uniform shift to the data.

A genetic algorithm (GA) (Goldberg 1989; Mitchell 1998) is used to generate initial estimates for the material parameters using a population size of 50 individuals (with 4–5 elites). For each individual, the 1-D Mulliken-Boyce model is calculated for each of the experimental conditions in the given data range. The fitness function (i.e., the figure of merit) of each individual for a given generation is calculated using a locally-converged value from a solution to the system of differential equations using a Levenberg-Marquardt least squares estimator (using MATLAB routines); the converged fitness value governs the likelihood of those estimates propagating to the next generation. The "optimal" estimate is the individual with the maximum fitness after a certain number of generations.

Using the GA-based 1D Mulliken-Boyce parameter estimator with local optimization, the best parameter estimates are obtained after 1000 generations, requiring several hours of run time on a multi-processor workstation. The results of the low strain rate parameter estimation are given in Table 3. The model predictions for low strain rates are plotted with the experiment data in Fig. 11. The agreement with the experiment data is excellent across the range of strain rates (0.0013 to 1.3 s^{-1}). The primary discrepancy is near the peak stress; the one-dimensional model presented in this paper predicts a sharp peak and sudden transition to softening, which is also seen in the three dimensional implementation by Mulliken and Boyce. However, the experimental data indicates a more gradual transition through the peak stress and to the subsequent softening. Hasan and Boyce's previous work (Hasan and Boyce 1995), utilizing a distribution function to describe the strained state of the material, qualitatively matches this gradual transition at the peak stress, which could indicate that a distribution function for the yield may need to be incorporated into the Mulliken-Boyce model to capture the transition. However, this was beyond the scope of the present work. Additionally, the total strain rate in the model is held constant at the average measured value of the strain rate in the experiment. This may result in additional error, particularly in the high strain rate experiments discussed in the next paragraph, where the total strain rate is not constant throughout the experiment duration.

We then hold the estimates from low strain rate data as constants and estimate the remaining parameters related to the β-transition from high strain rate data; these estimates are given in Table 4 and the model predictions and data are shown in Fig. 12. Qualitatively, the agreement between experiment and the model prediction is significantly worse

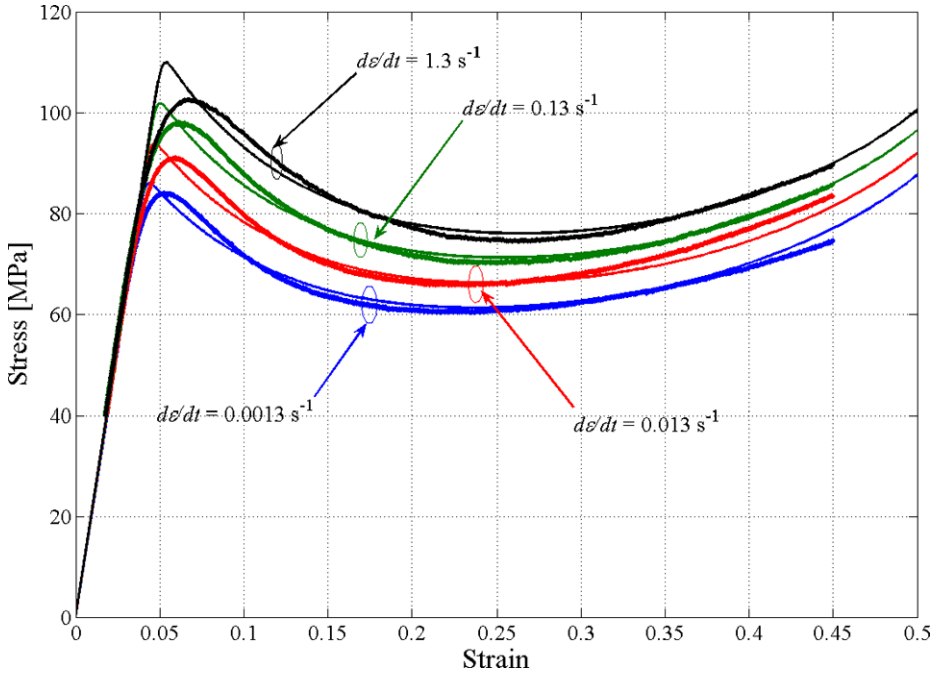

Fig. 11 The stress-strain relationship predicted from the 1-D Mulliken-Boyce model (*solid line*) using the parameter estimates in Table 3 for low strain rate. The experimental data (*heavy dotted line*) is plotted, showing the excellent agreement

Table 4 Parameter estimates from the high strain rate data

Symbol	$\dot{\gamma}_{0,\beta}$	ΔG_β	$\alpha_{p,\beta}$
Units	s^{-1}	J	–
Min	10	10^{-26}	0.01
Initial	10^5	10^{-25}	0.4
Final	1.55×10^7	4.32×10^{-20}	0.792
Max	10^{28}	10^{-17}	1

at high strain rates. While three-dimensional effects may partially explain the discrepancy, there are several other features that indicate other fundamental questions with respect to the β-transition. We begin by decomposing the stress-strain predictions from the model into the three stress components, i.e., the α, β, and Langevin stresses. These are plotted in Fig. 13. It is immediately evident that while the α stress contribution has a larger amplitude, the β stress contribution has a qualitatively different yielding behavior at high strain rate. This observation supports the differences in the evolution of the underlying physical processes as discussed and results in a β stress that is only significant at high strain rates. Without an intuitive model of the stress evolution from the equations alone, we perform a parametric sensitivity on the high strain rate data to diagnose the limitations of the model in Sect. 4.3. However, it should also be noted that the Mulliken-Boyce model was developed for amorphous polymeric materials, such as polycarbonate, whilst, epoxy is a ther-

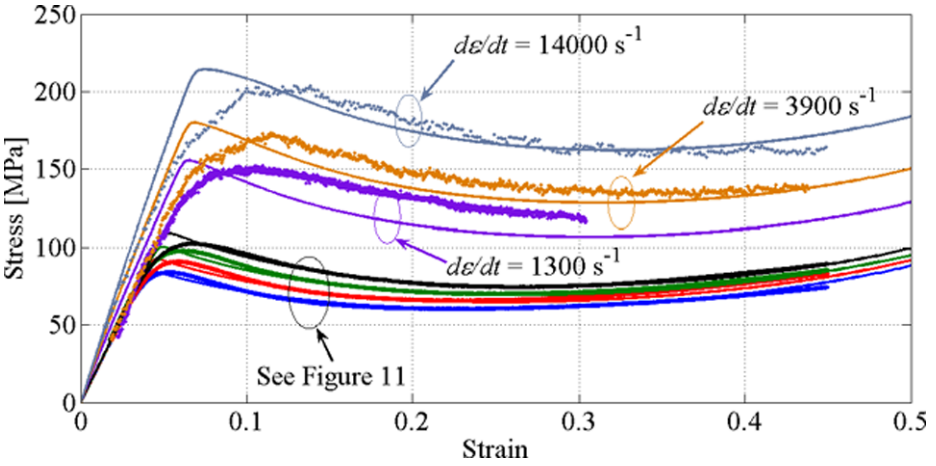

Fig. 12 Model predictions (*solid*) for the stress-strain dependence with a β-transition at high strain rates, holding the estimates from Table 3 as constants and including Table 4 estimates. The experimental data (*dotted*) is overlaid, showing only qualitative agreement at high strain rates

moset, crosslinked material. It has recently been shown in a comparison of polycarbonate and epoxy that the crosslinked material dissipates proportionally less work as heat (Garg et al. 2008). Since strain softening is modeled as being due to temperature rises that are in turn due to the conversion of mechanical work into heat, and because the model was developed for amorphous materials, we would anticipate that the strain softening predicted by the model would be greater than that observed in experimental epoxy specimens, and this is indeed the case.

4.3 Sensitivity analysis

The sensitivity of the model to changes in various parameters at a high strain rate ($\dot{\varepsilon} = 14000\ \mathrm{s}^{-1}$) is shown in Figs. 13 and 14. The parameters are explored about the final estimates. Three significant observations were made in the sensitivity analysis. The first is that the parameters related to the β transition, $\dot{\gamma}_{0,\beta}$, ΔG_β , and $\alpha_{p,\beta}$ (Fig. 13(b), (d), and (f), respectively), have a stronger influence than the corresponding α transitions for a similar perturbation. Variable sensitivity to different parameters is typical of ill-posed inverse problems, but a $\pm 1\%$ perturbation of ΔG_β or ΔG_β creates an exceptionally large change in the total stress in Fig. 13(d). The other observation is related to the stability of the solution. When higher perturbations (for example, $\pm 2\%$) were attempted on ΔG_α and ΔG_β , the differential equation became unstable and the solution failed. This implies two things: (1) great care must be taken in estimating the activation energy of the α- and β-transitions, and (2) there is a local region in parameter space where the solution is undefined. Correspondingly, there may be better estimates that are not able to be readily explored due to the discontinuous function. Another (independent) estimate or experimental measurement of the energy would also address this issue. The last observation is the physically high estimate for the β pressure coefficient ($\alpha_{p,\beta}$). Figure 13(e) and (f) show weak sensitivities to $\alpha_{p,\alpha}$ and $\alpha_{p,\beta}$, respectively; this implies that estimates of these underlying physical parameters are highly uncertain but also has a weak effect on the stress-strain relationships. Quantifying the exact uncertainty and covariances in the model is planned for future work.

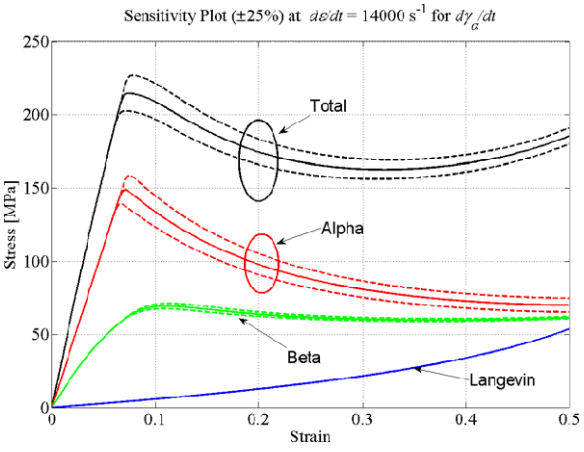

(a)

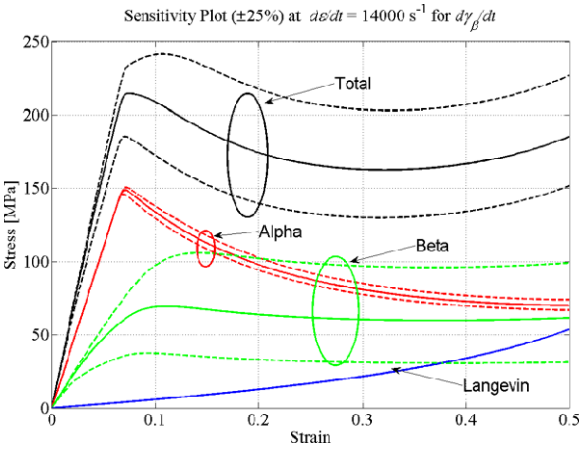

(b)

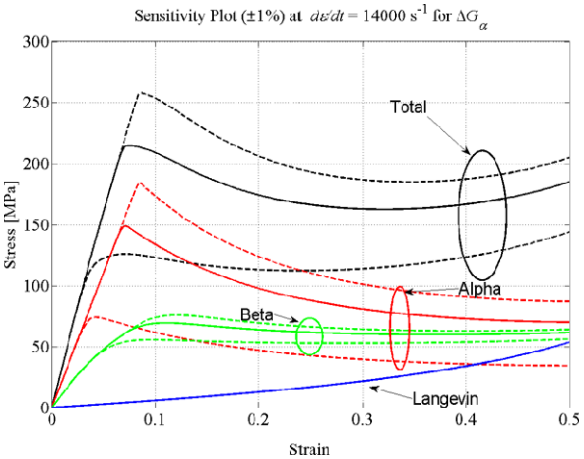

(c)

Fig. 13 Plots of the sensitivity of the model to percent changes in the various parameters; the dashed line is a positive change and the dotted line represents a negative change. The variables and levels adjusted are (**a**) $\dot{\gamma}_{0,\alpha}$ and (**b**) $\dot{\gamma}_{0,\beta}$ at ±25%, (**c**) ΔG_α and (**d**) ΔG_β at ±1%, and (**e**) $\alpha_{p,\alpha}$ and (**f**) $\alpha_{p,\beta}$ at ±10%

Fig. 13 (*Continued*)

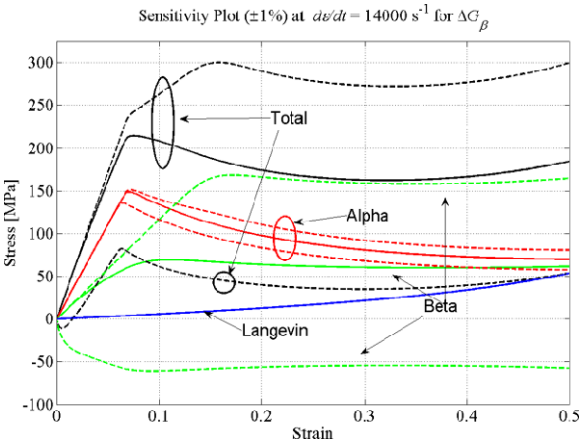

(d)

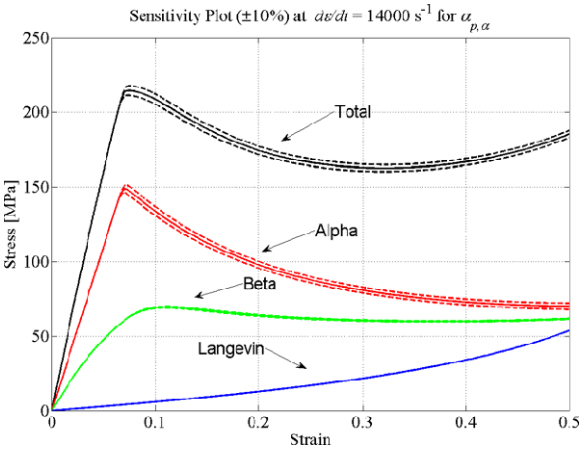

(e)

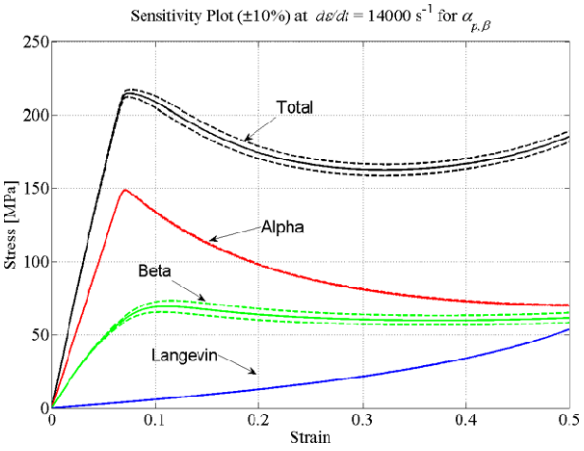

(f)

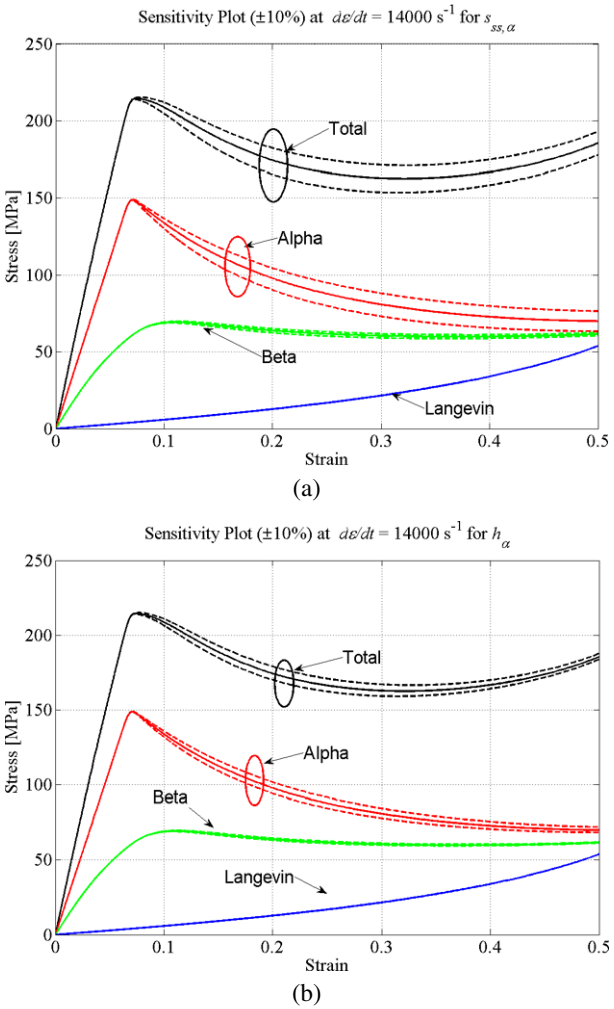

Fig. 14 Plots of the sensitivity of the model to changes in the various parameters; the dashed line is a positive change and the dotted line is a negative change. The variables are adjusted $\pm 10\%$ and are (**a**) $s_{ss,\alpha}$, (**b**) h_α, (**c**) C_R, and (**d**) N

5 Conclusions

The compressive mechanical properties of Epon 826 with diethanolamine hardener were measured in this study across a range of strain rates. An approximately bilinear dependence of yield stress on strain rate was observed and attributed to the β-transition in the epoxy, which was measured experimentally using dynamic mechanical analysis.

Interpreting a clear change peak stress vs. strain rate data as the onset of the β-transition, the estimates for a one-dimensional Mulliken-Boyce model were estimated using an sequential estimation approach. Low strain rate data was used to infer the model parameters for the α-transition and other properties. Excellent agreement between data and the model was obtained at low strain rates. High strain rate data was then used to develop estimates for the β-related parameters; significant discrepancies were observed. Sensitivity analysis was performed at the estimate to show the relative change in the model due to changes in the parameters.

Fig. 14 (*Continued*)

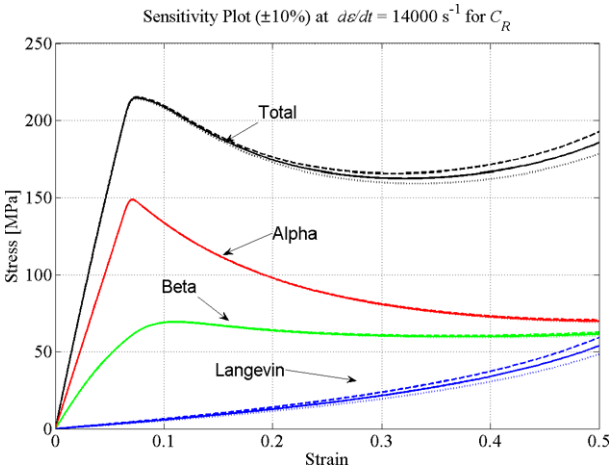

(c)

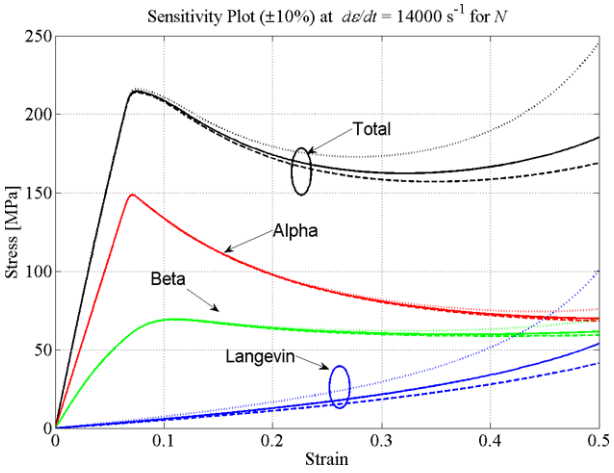

(d)

Acknowledgements The authors would like to acknowledge AFRL and AFOSR (Dr. Victor Giurgiutiu) for sponsoring this research. The authors would like to thank Mr. Wayne Richards, AFRL/RWME for preparing the epoxy material and Dr. David Williamson, Cavendish Laboratory, for conducting DMTA analysis.

Opinions, interpretations, conclusions, and recommendations are those of the authors and not necessarily endorsed by the United States Air Force.

References

Alifanov, O.M.: Inverse Heat Transfer Problems. Springer, Berlin (1994)

Anand, L., Ames, N.M.: On modeling the micro-indentation response of an amorphous polymer. Int. J. Plast. **22**(6), 1123–1170 (2006)

Arruda, E.M., Boyce, M.C.: Evolution of plastic anisotropy in amorphous polymers during finite straining. Int. J. Plast. **9**(6), 697–720 (1993)

Bar-Shalom, Y., Li, X.R., et al.: Estimation with Applications to Tracking and Navigation. Wiley, New York (2001)

Bauwens-Crowet, C.: The compression yield behaviour of PMMA over a wide range of temperature and strain-rates. J. Mater. Sci. **8**, 968–979 (1973)
Bauwens-Crowet, C., Bauwens, J.C., et al.: The temperature dependence of yield of polycarbonate in uniaxial compression and tensile tests. J. Mater. Sci. **7**, 176–183 (1972)
Bauwens, J.C.: Relation between the compression yield stress and the mechanical loss peak of bisphenol-A-polycarbonate in the β transition range. J. Mater. Sci. **7**, 577–584 (1972)
Bergstrom, J.S., Boyce, M.C.: Constitutive modeling of the large strain time-dependent behavior of elastomers. J. Mech. Phys. Solids **46**(5), 931–954 (1998)
Boyce, M.C., Kear, K., et al.: Deformation of thermoplastic vulcanizates. J. Mech. Phys. Solids **49**(5), 1073–1098 (2001)
Boyce, M.C., Parks, D.M., et al.: Large inelastic deformation of glassy polymers, part I: rate dependent constitutive model. Mech. Mater. **7**(1), 15–33 (1988)
Boyce, M.C., Socrate, S., et al.: Constitutive model for the finite deformation stress-strain behavior of poly(ethylene terephthalate) above the glass transition. Polymer **41**(6), 2183–2201 (2000)
Briscoe, B.J., Hutchings, I.M.: Impact yielding of high density polyethylene. Polymer **17**, 1099–1102 (1976)
Briscoe, B.J., Nosker, R.W.: The influence of interfacial friction on the deformation of high density polyethylene in a split Hopkinson pressure bar. Wear **95**, 241–262 (1984)
Briscoe, B.J., Nosker, R.W.: The flow stress of high density polyethylene at high rates of strain. Polym. Commun. **26**, 307–308 (1985)
Brown, E.N., Willms, R.B., et al.: Influence of molecular conformation on the constitutive response of polyethylene: a comparison of HDPE, UHMWPE, and PEX. Exp. Mech. **46** (2007)
Buckley, C.P., Dooling, P.J., et al.: Deformation of thermosetting resins at impact rates of strain, part 2: constitutive model with rejuvenation. J. Mech. Phys. Solids **52**(10), 2355–2377 (2004)
Buckley, C.P., Harding, J., et al.: Deformation of thermosetting resins at impact rates of strain, part I: Experimental study. J. Mech. Phys. Solids **49**(7), 1517–1538 (2001)
Chen, W., Lu, F., et al.: Tension and compression tests of two polymers under quasi-static and dynamic loading. Polym. Test. **21**(2), 113–121 (2002)
Chen, W., Zhang, X.: Dynamic response of Epon 828/T-403 under multiaxial loading at various temperatures. J. Eng. Mater. Technol. Trans. ASME **119**(3), 305–308 (1997)
Chen, W., Zhou, B.: Constitutive behavior of Epon 828/T-403 at various strain rates. Mech. Time-Depend. Mater. **2**(2), 103–111 (1998)
Chin, W., Hwu, J., et al.: Curing behavior and thermal properties of Epon 828 resin cured with diimide-diacid and phthalic anyhydride. Polymer **39**(20), 4923–4928 (1998)
Chou, S.C., Robertson, K.D., et al.: The effect of strain rate and heat developed during deformation on the stress-strain curve of plastics. Exp. Mech. **13**, 422–432 (1973)
Enns, J.B., Gillham, J.K.: Effect of the extent of cure on the modulus, glass transition, water absorption, and density of an amine-cured epoxy. J. Appl. Polym. Sci. **28**(9), 2831–2846 (1983)
Foreman, J.P., Porter, D., et al.: Thermodynamic and mechanical properties of amine-cured epoxy resins using group interaction modeling. J. Mater. Sci. **40**, 6631–6638 (2006)
Garg, M., Mulliken, A.D., et al.: Temperature rise in polymeric materials during high rate deformation. J. Appl. Mech. **75**, 011009-1–011009-8 (2008)
Gilat, A., Goldberg, R.K., et al.: Strain rate sensitivity of epoxy resin in tensile and shear loading. J. Aerospace Eng. **20**(2), 75–89 (2007)
Goldberg, D.E.: Genetic Algorithms in Search, Optimization, and Machine Learning. Addison Wesley, Boston (1989)
Gorham, D.A.: Measurement of stress-strain properties of strong metals at very high rates of strain. Inst. Phys. Conf. Ser. **47**, 16–24 (1979)
Gorham, D.A., Pope, P.H., et al.: An improved method for compressive stress strain measurement at very high strain rates. Proc. R. Soc. Lond. **438**, 153–170 (1992)
Gray III, G.T.: Classic split-Hopkinson pressure bar testing. In: Kuhn, H., Medlin, D. (eds.) Mechanical Testing and Evaluation. ASM Handbook, vol. 8, pp. 462–476. ASM International, Materials Park (2002)
Gray III, G.T., Blumenthal, W.R.: Split-Hopkinson pressure bar testing of soft materials. In: Kuhn, H., Medlin, D. (eds.) Mechanical Testing and Evaluation. ASM Handbook, vol. 8, pp. 488–496. ASM International, Materials Park (2000)
Hasan, O.A., Boyce, M.C.: A constitutive model for the nonlinear viscoelastic viscoplastic behavior of glassy polymers. Polym. Eng. Sci. **35**(4), 331–344 (1995)
Hu, Y., Xia, Z., et al.: Deformation behavior of an epoxy resin subject to multiaxial loadings, part I: experimental investigations. Polym. Eng. Sci. **43**(3), 721–733 (2003)
Jia, D., Ramesh, K.T.: A rigorous assessment of the benefits of miniaturization in the Kolsky bar system. Exp. Mech. **44**, 445–454 (2004)

Katz, D., Smooha, Y., et al.: Dynamic properties of an unfilled and filled epoxy resin subjected to extensional creep. J. Mater. Sci. **15**(5), 1167–1174 (1980)
Khan, M.Z.S., Simpson, G., et al.: A comparison of the mechanical properties in compression of two resin systems. Mater. Lett. **52**(3), 173–179 (2002)
Kozey, V., Kumar, S.: Compressive behavior of epoxy resins. In: International SAMPE Technical Conference (1994)
Kukureka, S.N., Hutchings, I.M.: Measurement of the mechanical properties of polymers at high strain rates by Taylor impact. In: Blazynski, T.Z. (ed.) Proc. 7th Int. Conf. on High Energy Rate Fabrication, pp. 29–38. University of Leeds, Leeds (1981)
Lu, H., Tan, G., et al.: Modeling of constitutive behavior for Epon 828/T-403 at high strain rates. Mech. Time-Depend. Mater. **5**(2), 119–130 (2001)
Mendenhall, W.: Introduction to Probability and Statistics, pp. 55–88. Duxbury, Belmont (1971)
Mentha, S.N., Pope, P.H., et al.: Progress in metal testing with a 3 mm pressure bar. Inst. Phys. Conf. Ser. **70**, 175–176 (1984)
Mitchell, M.: An Introduction to Genetic Algorithms. MIT Press, Cambridge (1998)
Miwa, M., Takeno, A., et al.: Strain rate and temperature dependence of shear properties of epoxy resin. J. Mater. Sci. **30**(7), 1760–1765 (1995)
Mulliken, A.D.: Low to high strain rate deformation of amorphous polymers: experiments and modeling. MSc thesis, Department of Mechanical Engineering. Cambridge, Massachusetts Institute of Technology (2004)
Mulliken, A.D.: Mechanics of amorphous polymers and polymer nanocomposites during high rate deformation. PhD thesis, Mechanical Engineering. Cambridge, Massachusetts Institute of Technology (2006)
Mulliken, A.D., Boyce, M.C.: Mechanics of the rate-dependent elastic-plastic deformation of glassy polymers from low to high strain rates. Int. J. Solids Struct. **43**(5), 1331–1356 (2006)
Mulliken, A.D., Soong, S.Y., et al.: High-rate thermomechanical behavior of poly(vinyl chloride) and plasticized poly(vinyl chloride). J. Phys. IV **134**, 217–223 (2006)
Rietsch, F., Bouette, B.: The compression yield behaviour of PC over a wide range of strain rates and temperatures. Eur. Polym. J. **26**, 1071–1075 (1990)
Siviour, C.R., Walley, S.M., et al.: The high strain rate compressive behavior of polycarbonate and polyvinylidene fluoride. Polymer **46**, 12546–12555 (2005)
Siviour, C.R., Walley, S.M., et al.: Mechanical behaviour of polymers at high rates of strain. J. Phys. IV **134**, 949–955 (2006)
Tasker, D.G., Dick, R.D., et al.: Mechanical properties of explosives under high deformation loading conditions. In: Shock Compression of Condensed Matter. American Institute of Physics, New York (1997)
Tasker, D.G., Dick, R.D., et al.: Mechanical properties of explosives under high deformation loading conditions. In: Shock Compression of Condensed Matter. American Institute of Physics, New York (1998)
Trautmann, A., Siviour, C.R., et al.: Lubrication of polycarbonate at cryogenic temperatures in the split Hopkinson pressure bar. Int. J. Impact Eng. **31**, 523–544 (2005)
Truong, V.T.: Effect of displacement rate and curing conditions on the fracture behaviour of crosslinked epoxy systems. Polymer **31**(9), 1669–1677 (1990)
Walley, S.M., Field, J.E.: Strain rate sensitivity of polymers in compression from low to high rates. DYMAT J. **1**(3), 211–227 (1994)
Williams, J.G.: The beta relaxation in epoxy resin-based networks. J. Appl. Polym. Sci. **23**, 3433–3444 (1979)
Xia, Z., Hu, Y., et al.: Deformation behavior of an epoxy resin subject to multiaxial loadings, part II: constitutive modeling and predictions. Polym. Eng. Sci. **43**(3), 734–748 (2003)